Physicochem. Probl. Miner. Process., 58(5), 2022, 156486

http://www.journalssystem.com/ppmp

Physicochemical Problems of Mineral Processing

ISSN 1643-1049

Multi-phase CFD modelling of slurry column flotation – validation of both hydrodynamic and kinetic parameters

P. Kopparthi [1,2], B. Vadlakonda[1], M. Kumar [1], N. Mangadoddy [1]

[1] Department of Chemical Engineering, Indian Institute of Technology Hyderabad, Kandi -502285, India

[2] Research & Development, Scientific Division, Tata Steel Ltd Jamshedpur -831001, India

Corresponding author: narasimha@che.iith.ac.in (Narasimha Mangadoddy)

Abstract: Column flotation is widely used for the beneficiation of fines in the mineral processing industry. The kinetics in the column flotation is mainly influenced by the hydrodynamics and the flotation sub-processes such as bubble particle collision, attachment, and detachment. Computational fluid dynamics (CFD) is a popular tool that can be used to evaluate flotation kinetics. However, most of the published works on the flotation kinetics with CFD were limited to mechanical flotation cells. In the current investigation, a CFD model is applied to explore both the hydrodynamics and kinetics of the column flotation. CFD simulations are performed for two-phase systems of column flotation on the Eulerian-Eulerian framework. The standard k-ε turbulence model is utilized in this methodology along with the drag, lift, and virtual mass forces. The hydrodynamic parameters such as axial, and radial gas holdup and its distribution were predicted from the CFD simulations and validated with Electrical Resistance Tomography (ERT) experimental results. In the kinetic study, the flotation kinetic sub-processes, such as bubble-particle collision, adhesion, and detachment were also predicted. The error between the ERT experimental and CFD simulations was found to be 2.71 and 6.75%, respectively at 0.006 and 0.018 m/s superficial air velocities. The effect of particle contact angle and particle size on the kinetic constants of attachment (k_1) was evaluated and was found to increase with the contact angle. The rate of attached particle fraction is found to increase from 40 to 100 μm and to decrease to 250 μm. The CFD model predictions were found to be consistent with the experimental results of the weakly floatable coal particles.

Keywords: column flotation, hydrodynamics, bubble size distribution, gas holdup, eulerian–eulerian model, solids concentration and kinetics

1. Introduction

The development of column flotation is one of the most significant achievements in the mineral processing industry in the 20th century. High recoveries are made possible with column flotation compared to conventional cells. This is due to the counter-current contact between the descending solid particles and rising air bubbles in the aqueous phase coupled with the froth-washing system. The air bubbles are dispersed into the liquid column via a sparger from the bottom, whereas the feed solid particles are fed just above the middle point of the column. The column has two different zones, namely the collection zone and the cleaning zone. The collection zone is below the feed point and above the sparger region where the bubble-particle attachment occurs. The bubble-particle aggregates then move to the top section of the column, above the feeding point, named the cleaning zone. The wash water in the cleaning zone removes the entrained gangue particles from the product, leading to higher purity of the product. The hydrophilic particles are discharged from the bottom as tailings.

Although the basic concept of a flotation column appears to be simple, the fundamental principles related to its performance are rather complex. The flotation separation process is mainly influenced by surface chemistry and hydrodynamics. The solid suspension and the aggregate transport are controlled by the hydrodynamic characteristics, which have an impact on the design, optimization, and flotation performance (Prakash *et al.*, 2018). Finch & Dobby, (1990) proposed an empirical relationship to predict

DOI: 10.37190/ppmp/156486

the bubble size from the superficial gas velocity for the uniform bubbles. Vazirizadeh *et al.*, (2015) introduced the interfacial area of bubbles to get more information about the size distribution and it was modelled using log-normal bubble size distributions rather than a single average bubble size d_{32}. Panjipour *et al.*, (2021) developed a relation between the interfacial area of the bubbles, the bubble size distribution, and the flotation kinetics in a pilot column flotation. Finch *et al.*, (2000) established the linear relationship between the bubble surface area flux and the gas holdup for various flow regimes. Vadlakonda & Mangadoddy, (2017) have measured the key hydrodynamic parameters such as sectional average and radial average gas holdup, Sauter mean bubble diameter, and bubble rise velocity in the column flotation experimentally by electrical resistance tomography (ERT). Also, many researchers have worked on the slurry column flotation hydrodynamics (Banisi *et al.*, 1995; Tavera *et al.*, 2001; Tavera & Escudero, 2002; Mena *et al.*, 2005; Bhunia *et al.*, 2015). The minimal change was found to occur in the bubble size with the increase in the solids percent, both hydrophilic and hydrophobic particles, in the slurry. Vadlakonda & Mangadoddy, (2018) studied the effect of solids on the gas holdup and its dispersion in the three-phase column. The gas holdup decreased with the addition of solids in the column flotation. The influence of operational parameters such as superficial velocities of air and feed, different porous spargers, pulp height, and frother dosage on the combined (gas and solid) holdup and its distribution were also investigated. According to Honaker & Mohanty, (1996) and Ahmed & Jameson, (1989), higher gas holdup should improve the flotation kinetics due to a greater number of bubbles per unit volume of slurry. Yianatos *et al.*, (2017) discovered that the mixing regime in flotation columns could not be characterised by a single model structure, nor could it be related to column cross-sectional shapes or size.

A computational fluid dynamics (CFD) model was used earlier by several researchers to investigate the hydrodynamics and kinetics of the flotation process independently. In flotation kinetics, the necessary step for a successful bubble-particle collection process is the bubble-particle collision. Koh *et al.*, (2000) evaluated the distribution of bubble-particle collision frequency in the CSIRO flotation cell using CFD. It was reported that the maximum collision rates were observed near the rotor-stator region. The efficient capture of hydrophobic particles by air bubbles is accomplished in three sub-processes: the probability of collision, probability of adhesion, and probability of stability. The probability of bubble-particle collision was modelled using CFD by Koh & Schwarz, (2003) who reported that collision probability decreased with particle size and increased with bubble size. Later, the three sub-processes: the probability of collision, probability of attachment, and probability of detachment were determined using the CFD modelling in a CSIRO flotation cell. It was observed that the predicted flotation rate was maximum for intermediate size particles (120-240 μm) compared to fine (40 μm) and coarse (480 μm) particles (Koh & Schwarz, 2006). These simulation studies were carried out for a constant bubble size. Multi-size bubbles were introduced through the population balance method (PBM) and the bubble-particle attachment rates in a Denver flotation cell were predicted in the CFD simulation studies for constant particle size. It was also reported that for a given particle size, a maximum flotation rate exists for a particular bubble size (Koh & Schwarz, 2008). The bubble-particle collision efficiency was calculated in a Lagrangian approach in a turbulent field (Liu & Schwarz, 2009). Karimi *et al.*, (2014) developed a CFD model to predict the flotation rate constant in a standard Rushton turbine flotation cell using the Eulerian-Eulerian approach. It was reported that the flotation rate constant increased with particle size for an increase in the superficial air velocity.

For column flotation, most of the published literature focused on the hydrodynamics of column flotation. Sarhan *et al.*, (2016) studied the impact of gas superficial velocity and solids concentration on Sauter mean bubble diameter and gas holdup. Sarhan *et al.*, (2017) investigated the effect of solids particles (type, density, and concentration) on gas holdup and hydrodynamics. It was reported that, for two-phase systems, the gas holdup increased linearly with the superficial air velocity. For the three-phase system, the gas holdup increased in the presence of of hydrophilic particles and decreased in the presence of hydrophobic particles in column flotation. The developed CFD model predicted the gas holdup with+/-20% acuracy. Mwandawande *et al.*, (2019) investigated the gas holdup and its deviation in the collection zone in the gas-liquid flow of the column. With the increasing column height, the axial velocity of the air bubbles decreased. From the literature review, it is evident that most of the published CFD models on the evaluation of flotation kinetics were focused on the mechanical flotation cells and

for column flotation, the studies were restricted to hydrodynamic studies only. The current study aimed to develop a CFD model strategy incorporating both hydrodynamics and kinetics of the column flotation thereby attempting to validate key performance parameters. Numerical simulations were performed for two-phase and three-phase systems of column flotation based on the Eulerian-Eulerian framework. The intended model utilizes the k-ε turbulence model along with the drag, lift, and virtual mass hydrodynamic forces. Further, the predicted hydrodynamic parameters are validated with ERT experimental data. The bubble-particle collision, bubble-particle adhesion, and bubble-particle detachment were also considered in the kinetic study of the column flotation process. A parametric study on coal particle contact angle and particle size was carried out and the key kinetic performance of the column flotation was elucidated.

2. CFD modelling

Column flotation, which was previously employed for the ERT tests by the authors (Vadlakonda & Mangadoddy, 2017), was used for the CFD modelling in this work. The column used in the test was of diameter 0.1 m and height 2.5 m. The sparger geometry was created and meshed based on the porosity values of the sparger.

2.1. Model for hydrodynamics

The two-fluid model (Eulerian - Eulerian) was used in the simulation studies of column flotation. The gas-liquid phases interact with each other in a two-fluid model method, where there is significant mass and momentum exchange between the phases. The interphase forces such as drag, lift, and virtual mass were considered in the numerical simulations. Tomiyama, (1998) model was used to model the lift force. Ishii & Zuber, (1979) drag model was considered for the gas-liquid phase drag force, while Schiller and Naumaan, (1935) drag model was used for the solid-liquid phase drag force in the three-phase numerical simulations. The k-ε turbulence model was used to consider the turbulence between the phases. Despite the limitations, the k-ε model is computationally cheap, robust, and has a good convergence rate. It is also easy to implement and widely validated. The bubble-bubble interactions were considered by the population balance model (PBM). The break-up model from Luo & Svendsen, (1996) and the coalescence process Luo, (1993) aggregation kernel were used.

2.1.1. Eulerian-Eulerian Two fluid model

- Continuity equation:

$$\frac{\partial}{\partial t}\left(\alpha_q \rho_q\right) + \nabla.\left(\alpha_q \rho_q \vec{v}_q\right) = 0 \tag{1}$$

The compatibility condition for two-phase volume fractions, $\alpha_p + \alpha_q = 1$

- Momentum equation:

$$\frac{\partial}{\partial t}\left(\alpha_q \rho_q \vec{v}_q\right) + \nabla.\left(\alpha_q \rho_q \vec{v}_q \vec{v}_q\right) = -\alpha_q \nabla p + \nabla.\bar{\bar{\tau}}_q + \alpha_q \rho_q \vec{g} + \sum_{p=1}^{n}\left(\vec{R}_{pq} + \dot{m}_{pq}\vec{v}_{pq} - \dot{m}_{qp}\vec{v}_{qp}\right) + \\ +\left(\vec{F}_q + \vec{F}_{lift,q} + \vec{F}_{vm,q}\right) \tag{2}$$

- The stress tensor:

$$\bar{\bar{\tau}}_q = \alpha_q \mu_q\left(\nabla \vec{v}_q + \nabla \vec{v}_q^T\right) + \alpha_q\left(\lambda_q - \frac{2}{3}\mu_q\right)\nabla.\vec{v}_q I^{=} \tag{3}$$

- Interaction force between phases

$$\sum_{p=1}^{n} \vec{R}_{pq} = \sum_{p=1}^{n} K_{pq}\left(\vec{v}_p - \vec{v}_q\right) \tag{4}$$

- Interphase momentum exchange coefficient:

$$K_{pq} = \frac{\propto_p \propto_q \rho_p f}{\tau_p} \tag{5}$$

- Drag function:

$$f = \frac{C_D Re}{24} \tag{6}$$

$$\mathrm{C_D} = \frac{24}{Re_B}(1 + 0.1Re^{0.75}) \qquad \text{(Viscous region)} \tag{6.1}$$

$$C_D = 0.44\mathrm{E} \quad \text{(Newton regime)} \tag{6.2}$$

$$C_D = \frac{2}{3}\sqrt{\mathrm{E_O}}\,E \quad \text{(Distorted regime)} \tag{6.3}$$

$$C_D = \frac{8}{3}E' \quad \text{(Churn-turbulent regime)} \tag{6.4}$$

- Particulate relaxation time:

$$\tau_p = \frac{\rho_p d_p^2}{18\mu_q} \tag{7}$$

- The lift force calculated as:

$$\vec{F}_{lift} = C_L\rho_q\alpha_p\left(\vec{v}_q - \vec{v}_p\right)\times\left(\nabla\times\vec{v}_q\right) \tag{8}$$

- The virtual mass force on the bubbles:

$$\vec{F}_{vm} = C_{VM}\rho_q\alpha_p\left(\frac{d_q\vec{v}_q}{dt} - \frac{d_p\vec{v}_p}{dt}\right) \tag{9}$$

2.2. Model for kinetics

Flotation kinetics is modelled through applying source terms in the transport equation for the concentration of particles. In the current investigation, the approach is used here similar to Koh & Schwarz, (2006).

2.2.1. Flotation Kinetics Equations

- Transfer of particles from pulp to bubbles represented by scalar transport equation:

$$\frac{\partial}{\partial t}\left(\alpha_q n_q \emptyset_q\right) + \nabla\cdot\left(\alpha_q n_q \emptyset_q \overrightarrow{u_q}\right) = -\varphi_a + \varphi_d \tag{10}$$

- For the flotation, the kinetic equation can be written as:

$$\frac{\mathrm{dN_{p1}}}{\mathrm{dt}} = -\mathrm{k_1 N_{p1} N_{bT}}(1-\beta) + \mathrm{k_2 N_{bT}}\beta \tag{11}$$

- Bubble loading:

$$\beta = \frac{n_{p2}}{2\left(\frac{d_{32}}{d_{sp}}\right)^2 n_{bT}} \tag{12}$$

- The kinetic constant of attachment:

$$\mathrm{k_1} = \mathrm{Z_1 P_c P_a P_s} \tag{13}$$

- The kinetic constant of detachment:

$$\mathrm{k_2} = \mathrm{Z_2}(1-\mathrm{P_s}) \tag{14}$$

- The particle–bubble collision frequency (Z_1) across eddies»

$$Z_1 = 5.0\left(\frac{d_p+d_b}{2}\right)^2\left(\vec{u}_p^2 + \vec{u}_b^2\right)^{\frac{1}{2}} \tag{15}$$

- The rms velocity of particle or bubble (Liepe & Mockel, 1976) are given by:

$$U_p = \frac{0.4\varepsilon^{\frac{4}{9}}d_p^{\frac{7}{9}}}{v_f^{\frac{1}{3}}}\left(\frac{\rho_p-\rho_f}{\rho_f}\right)^{\frac{2}{3}} \quad \text{and} \quad U_b = \frac{0.4\varepsilon^{\frac{4}{9}}d_b^{\frac{7}{9}}}{v_f^{\frac{1}{3}}}\left(\frac{|\rho_b-\rho_f|}{\rho_f}\right)^{\frac{2}{3}} \tag{16}$$

- The critical diameter (d_{cr}) of a particle or bubble, is given by:

$$d_p^2 > d_{cr}^2 = \frac{15v_f\rho_f u_f^2}{\rho_p\varepsilon} \quad \text{and} \quad d_b^2 > d_{cr}^2 = \frac{15v_f\rho_f u_f^2}{\rho_b\varepsilon} \tag{17}$$

- The collision efficiency (Z_1) for fine particles and bubbles confined within eddies in the lower turbulent dissipation regions (Saffman & Turner, 1956):

$$Z_1 = \sqrt{\frac{8\pi}{15}}\left(\frac{d_p+d_b}{2}\right)^3\left(\frac{\varepsilon}{\vartheta}\right)^{\frac{1}{2}} \tag{18}$$

- The detachment frequency (Z_2):

$$Z_2 = \frac{\sqrt{C_1 \varepsilon^{\frac{1}{3}}}}{(d_p+d_b)^{\frac{2}{3}}} \quad 9)$$

- The bubble – particle collision:

$$P_c = \left[1.5 + \frac{4Re^{0.72}}{15}\right]\left(\frac{d_p}{d_b}\right)^2 \quad (20)$$

- For intermediate bubble Reynolds number:

$$\mathrm{Re} = \frac{u_b d_b}{v_f} \quad (21)$$

- The probability of adhesion:

$$P_a = sin^2\left[2exp\left\{\frac{-(45+8Re^{0.72})u_{b,}t_{ind}}{15d_b\left(\frac{d_b}{d_p}+1\right)}\right\}\right] \quad (22)$$

- The induction time:

$$t_{ind} = \frac{75}{\theta} d_p^{0.6} \quad (23)$$

- The probability of stability:

$$(P_s) = 1 - exp\left\{0.5 * \left(1 - \frac{1}{Bo^*}\right)\right\} \quad (24)$$

- The modified Bond number:

$$Bo^* = \frac{d_p^2\left[\Delta\rho_p g + 1.9\rho_p \varepsilon^{\frac{2}{3}}\left(\frac{d_p}{2}+\frac{d_b}{2}\right)^{-\frac{1}{3}}\right] + 1.5d_p\left(\frac{4\sigma}{d_b} - d_b\rho_f g\right)sin^2\left(\pi-\frac{\theta}{2}\right)}{\left|6\sigma sin\left(\pi-\frac{\theta}{2}\right)sin\left(\pi+\frac{\theta}{2}\right)\right|} \quad (25)$$

2.3. Geometry, mesh and numerics

ANSYS Fluent commercial CFD software, version 19.2 was utilised for this study. The ICEM-ANSYS was currently used to develop the 3D unstructured grid for the column, displayed in Figure 1. The hex mesh of the column and O grid of outlet sections are shown in Figs. 1(b) and (c), respectively. The unstructured mesh was used for the inlet section of the column. The bubble interactions are mainly considered via the population balance model (PBM) approach in the simulations. Air is injected into the system at 0.006, 0.012, and 0.018 m/s superficial velocities via a sintered disc sparger. Column simulations were performed at a feed velocity of 0.0004 m/s, 2.4 m pulp height, and 60,000 pore density spargers. Initially, a bubble size of 0.0025 m, as observed in experiments, is used in the simulations. A velocity inlet boundary condition is used at the gas inlet and the degassing boundary condition is applied at the exit condition of the column. In the transient mode, the time step of 0.0001 s was used. The phase-coupled SIMPLE algorithm with a QUICK scheme was used for the pressure-velocity coupling in the numerical simulations. Different mesh size having nodes in the range of 90-260k were utilized for the grid independence study of laboratory flotation column simulations.

The average gas holdup was chosen for the mesh independence test. The grid independence test was carried out with five different meshes i.e., 90,460, 117,864, 150,386, 200,725, and 259,657 nodes and corresponding two-phase flow results are displayed in Figure 2. Average radial gas distribution profiles are evaluated for 0.006, 0.012, and 0.018 m/s air superficial velocities at 0.9 m elevation from the column's bottom. From Fig. 2, it was found that 90,460 and 117,864 mesh nodes are under-predicting the average radial holdup values at three air superficial velocities compared to experimental data. 150,386, 200,725, and 259,657 grid's predicted gas holdup outcomes closely match the experimental data. As the computational time increases linearly as the mesh size increases, 150, 386 nodes (mesh 3) was chosen as the optimum grid to run further simulations.

3. Results and discussion

CFD-based two-phase studies are initially attempted to comprehend the hydrodynamics of multi-phase flow. The three-phase flow simulations are carried out further, by considering hydrophilic silica as a solid phase in the CFD simulations. The phase concentration distribution and bubble-particles interactions are essential for improving the design and selection of suitable column flotation for a given

nature of particle floatability and kinetics information. The bubble-particle collision, attachment, detachment, and stability probability are predicted at different contact angles of coal particles as part of three-phase flow predictions.

3.1. Hydrodynamic model prediction & validation

The population balance model (PBM) is used for predicting the bubble-bubble interactions in the two-phase flow behaviour.

3.1.1. Two-phase simulations

Figure 3 (a) shows the impact of superficial air velocity on the overall gas holdup. The displayed results were at a height of 0.9 m from the bottom of the column. When the superficial air velocity is increased from 0.006 m/s to 0.018 m/s, the average gas holdup increased from 1.58 to 5.0%. The CFD simulation values were validated against ERT experimental data. The gas holdup at low superficial air velocity is matching very well with the ERT experimental data. At high superficial air velocities, the CFD predicted average gas holdup is slightly deviating from the experiments.

Figure 3 (b) presents a contour comparison of average pressure and liquid velocities for the column operated at 0.006 m/s and 0.018 m/s superficial air velocities. When the superficial air velocity is increased from 0.006 m/s to 0.018 m/s, the average pressure & liquid velocity also increased axially. At higher superficial air velocity, say at 0.018 m/s, the gross liquid circulations are enhanced due to dominant bubble interactions and oscillatory bubble plume nature. The same is witnessed in Fig. 4, where the axial variation of the bubble number density fraction is presented.

The predicted bubble number density fraction with different air superficial velocities at different axial locations are displayed in Figs. 4 (a) & (b). Small size bubbles are observed at the lower axial position with low air superficial velocity. As axial height increases, the coalescence phenomena start

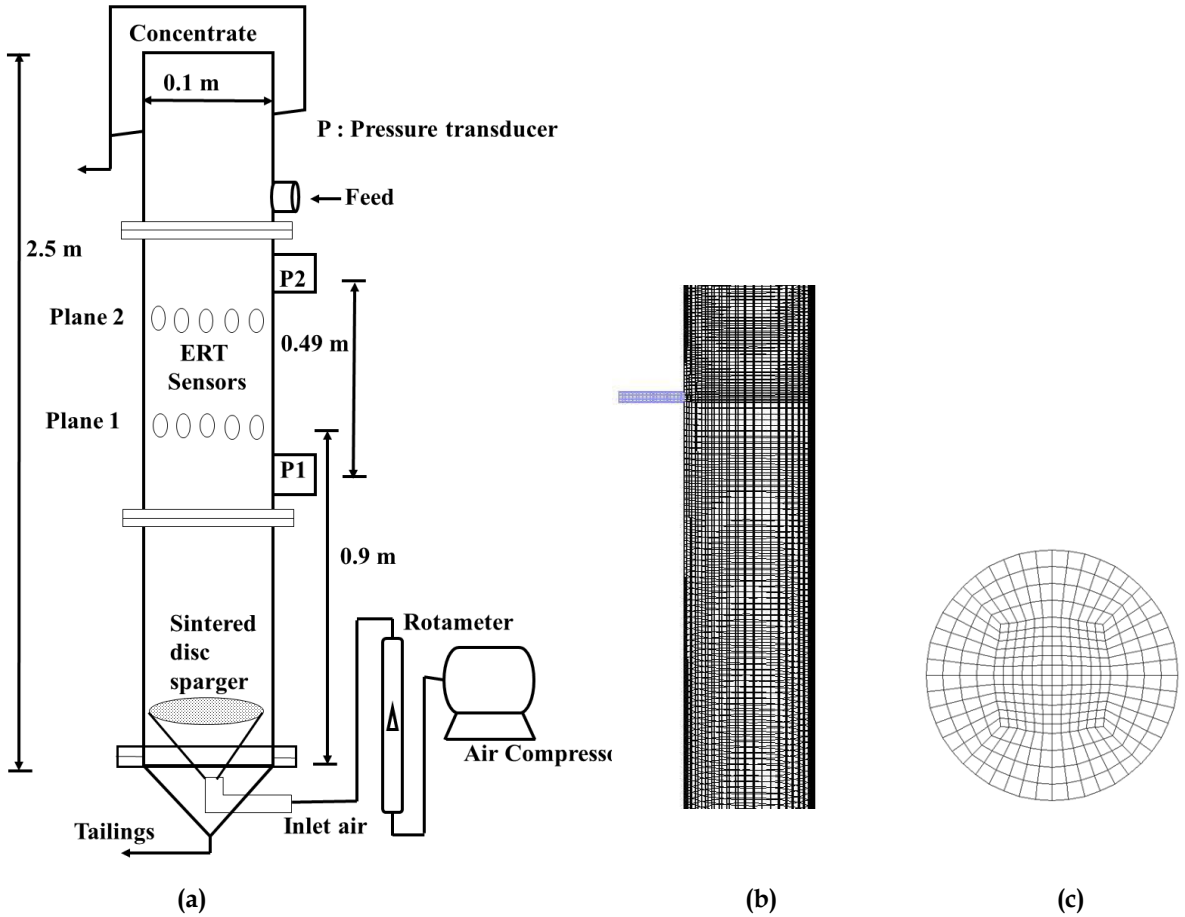

Fig. 1. (a) Experimental column with ERT (b) column cylindrical section mesh (c) column outlet

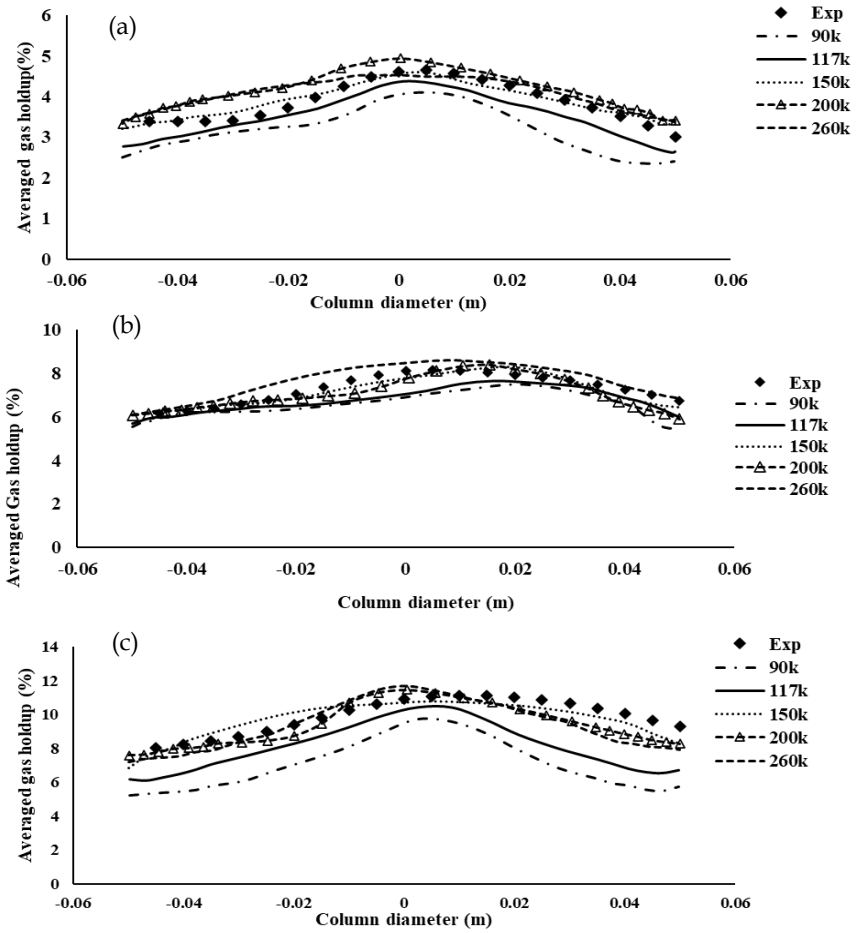

Fig. 2. Grid independence check with different grids averaged gas holdup at several air velocities (a) 0.006 m/s (b) 0.012 m/s (c) 0.018 m/s

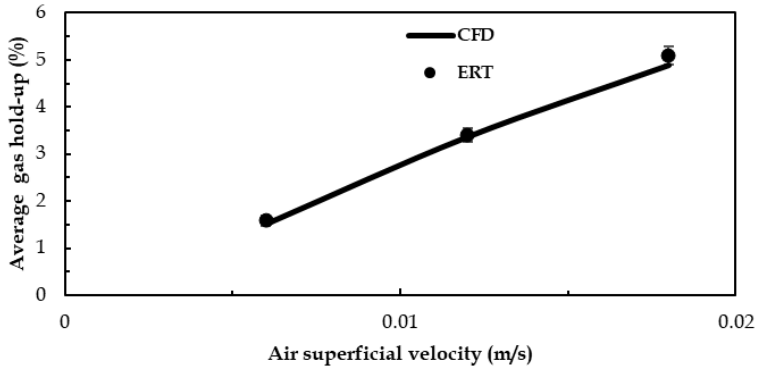

Fig. 3 (a).Comparison of sectional average gas holdup between CFD and ERT at different superficial air velocities

dominating and large size bubbles may also appear in the column. At low air superficial velocity, the bubble density fraction is relatively unchanged throughout the column except near the feed port region (H=1.5 m). The continuous incoming liquid flow creates some local turbulence and these interact with the bubbles thus leading to the possibility of bubble breakup. This generates smaller bubbles but with increased finer fractions. As the air superficial velocity increases, increments in the bubble interactions are observed axially in the column. At 0.018 m/s, near the sparger zone (at H=0.1 m), the number density fraction shows a perfect normal distribution with a mean bubble size of 0.004 m. As the height of the column increases, the mean and mode of the bubble size distribution (BSD) reduces, and this is believed due to increased bubble break-up and coalescence rates. Hence, the appearance of smaller and larger bubbles at 0.9 and 1.5 m axial positions of the column.

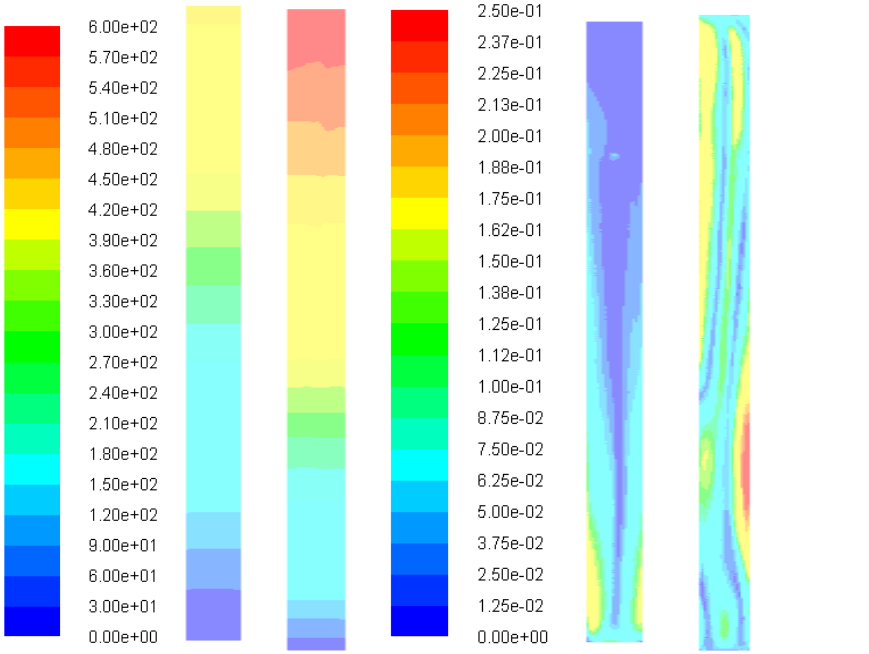

Fig. 3 (b).Comparison of average pressure and liquid velocities at 0.006 m/s and 0.018 m/s superficial air velocities

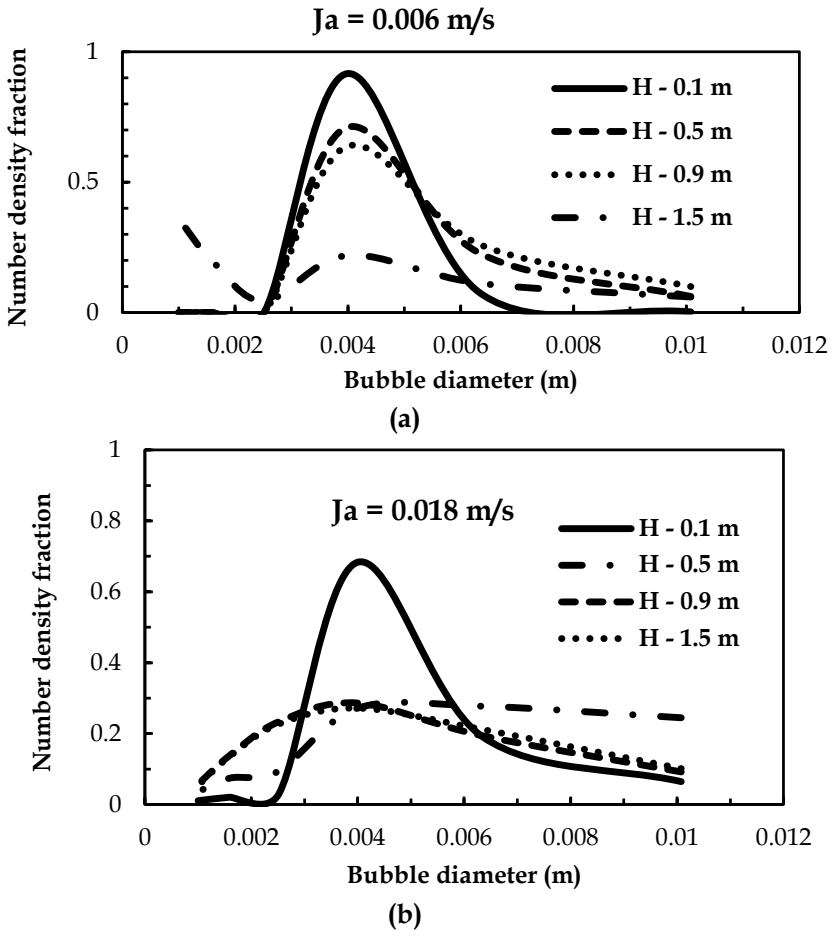

Fig. 4. Number density fraction at different axial lengths and air superficial velocity (a) 0.006 (b) 0.018 m/s

Apart from the sectional average gas holdup, Fig. 5 shows the radial profiles used to validate with ERT data. It is observed that predicted CFD values are closely matching with the ERT data at low superficial air velocities and slight deviations are observed at high velocities. The gas holdup is uniform at low air superficial velocity across the column due to the uniform distribution of bubbles. The bubbles occupy the center region instead of dispersion across the cross-section of the column at high air superficial velocities. The bubble break-up and coalescence phenomena dominate in increasing the gas hold-up at the center region of the column (Shah *et al*., 1982). From Fig. 5, it is observed that gas holdup increases significantly with superficial air velocity in both the experimental and the CFD simulation data. The error between the ERT experimental and numerical predictions for 60 k pores sparger at the centre and wall regions are 2.71 & 6.75%, respectively at 0.018 m/s superficial air velocity, whereas the error is 9.2 & 24.23% at 0.006 m/s superficial air velocity.

3.1.2. Three-phase simulations

Three-phase CFD simulations are performed using the Eulerian – Eulerian approach for the three feed solids scenarios i.e., 5, 10, and 15 wt.% silica in the solution. The simulations are carried out at 2.4 m pulp height, 0.004 m/s feed velocity, and 200 k pore number sparger. Figure 6 (a) shows the sectional averaged combined hold-up for different percent solids and superficial air velocities. The predicted numerical simulation phase holdup values were validated with the ERT experimental data. The predicted combined holdup increased with the superficial air velocity and the solids content, similar to

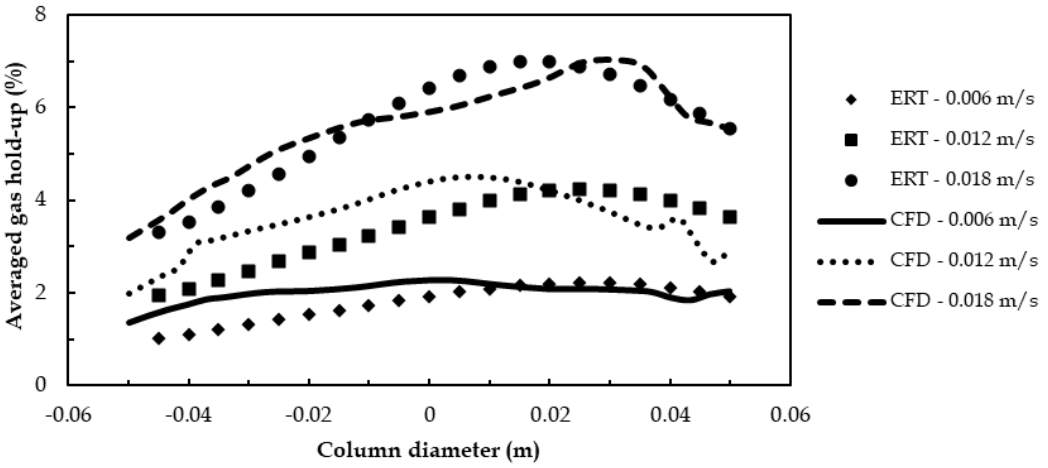

Fig. 5. Radial gas dispersion at diverse superficial air velocities

the experiments. A slight deviation was observed in the predicted CFD values compared to the experimental data at the high superficial air velocity of 0.018 m/s. The error between the predicted and experimental values at 0.018 m/s superficial air velocity for 5, 10, and 15 wt.% slurry solutions were 4.10, 5.30, and 6.06%, respectively. The predicted solids holdup is displayed in Fig. 6 (b) along with the ERT-coupled PT-based experimental data. It is observed that the change in the solids holdup with superficial air velocity is minimal. Generally, the probability of bubble-particle interactions increases with the superficial air velocity. But, the bubble-particle attachment rate is expected to be very low for hydrophilic solid particles. Hence the effect of superficial air velocity on the solids holdup is not significant as compared to hydrophobic slurry solution cases. Figure 6 (c) displays the comparison of predicted gas holdup values with the experimental data at various superficial air velocities and solids concentrations. Both CFD and experimental data demonstrated that the gas holdup decreases with solids content and increased with superficial air velocity. From the current study, both based on the experimental and the CFD studies, it is found that gas holdup decreases with solids concentration. The predicted gas holdup values are slightly deviating at 0.018 m/s superficial air velocity. The bubble interactions were not predicted well within the current PBM model at high superficial air velocity. The error between the predicted and the ERT experimental values at 0.018 m/s superficial air velocity for 5, 10, and 15 wt.% slurry solutions are 3.65, 7.10, and 7.55%, respectively. The average gas holdup increases

with the superficial air velocity linearly, where the flow is believed to be in the homogeneous flow regime. After that, the gas holdup follows a non-linear trend with the superficial air velocity in the transition and heterogeneous flow regimes.

3.2. Kinetic model

The Pyke et al. (2003) and Koh & Schwarz (2006) models have been used in the present numerical simulations as part of the flotation kinetic study. The first-order rate process of flotation is mainly dependent on the number of particles and bubbles in the bubble-particle attachment and detachment steps. The Shukla et al. (2010) laboratory column flotation with 0.1 m diameter and 1.68 m height is selected for the kinetic model studies. The mono-size bubbles having 0.0025 m are injected as the dispersed phase from the sparger located at the centre of the column with 0.003 m diameter and coal experimental data are utilized for the comparison. A uniform particle size of 40 μm and superficial air velocities of 0.0094, 0.0168, 0.0247, 0.0329, 0.0414, and 0.0527 m/s are used in the numerical simulations. Figure 7 presents the gas holdup variation to the superficial air velocities for the coal slurry operating similarly to silica slurry. The coal slurry gas holdup increases linearly with superficial gas velocity. At higher gas velocities, column operation getting into a heterogeneous flow regime can be attributed to the coalescence of the small bubbles leading to relatively lower gas holdups (Shah *et al.*, 1982; Vadlakonda and Mangadoddy 2018; Finch and Dobby, 1990).

The probabilities of collision, attachment, and stability have been simulated at 30^0 and 70^0 contact angles, and the same is presented in Fig. 8. It is observed that collisional probability is more at 70^0 contact angle. At a higher contact angle, say at 70^0, the hydrophobic nature has increased and as a result, an increase in the attachment fraction and a decrease in the detachment fraction were observed. The attachment probability and air volume fraction are higher at the centre region compared to the walls in

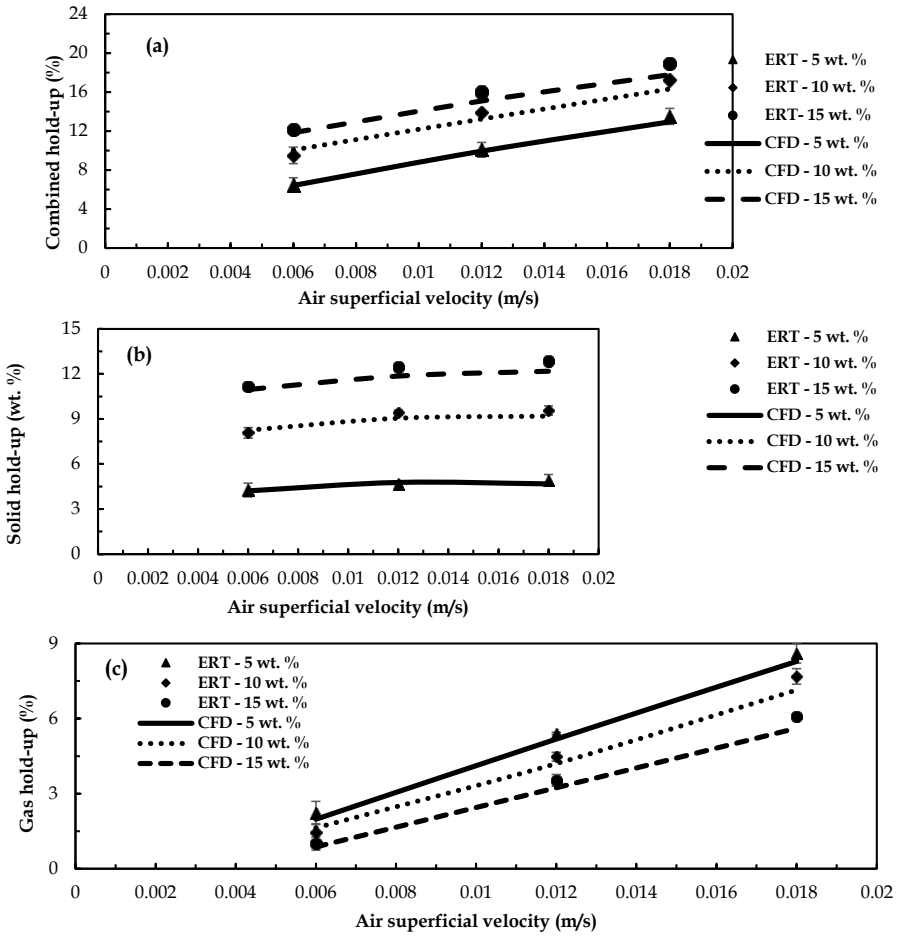

Fig. 6. (a) Comparison of predicted combined holdup (b) solid holdup (c) gas holdup values with ERT experimental data at different solids and superficial air velocity

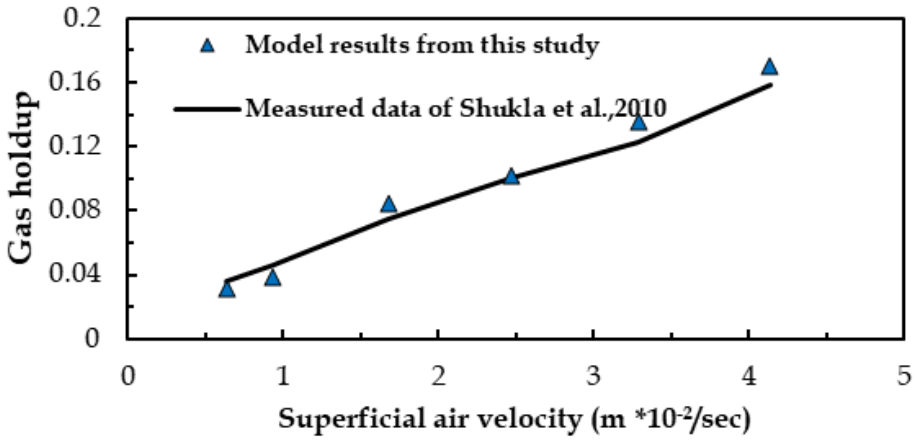

Fig. 7. Gas holdup values at different superficial air velocities

the column. Similar to the gas holdup, the collision probability and stability probability were found higher in the column centre compared to the wall region. As the bubble plume behavior follows an oscillatory trend, the probability of collision and stability also follow a similar radial variation. The attachment rate constants values are also predicted at 30^0 and 70^0 contact angles. The average attachment rate constant values are 0.054 and 0.159 s^{-1} at 30^0 and 70^0 contact angles respectively. The radial distribution of the attachment rate constant at different contact angles is presented in Fig. 9. The radial distribution of the attachment rate is found to increase with the contact angle. As a result, the attachment rate will increase, and the process performance is also expected to increase. The particle collection efficiency also increases with the contact angle.

The comparison of the bubble-particle attachment rate constant (K_1) values at the contact angle (70^0) is displayed along with the experimentally determined data (Shukla, 2010) in Table 1. The bubble-particle attachment rate constant depends on the particle size. The attachment efficiency is more for the small size particles. The experimental value presented in the table are for the 150 µm particle size particle and the predicted CFD value are for the 40 µm particle size. The bubble-particle attachment rate constant increases with a decrease in the particle size. Hence the predicted CFD values are in principle agreement with experimental data. Further studies are in pipeline to incorporate slurry rheology and turbulent dispersion forces on the net rate of attachment and detachment of particles on bubbles.

Table 1. Comparison of bubble-particle attachment rate constant (K_1) value

	Bubble-particle attachment rate constant (K_1) (m^{-1})
Experimental data	0.025
CFD data	0.042

Using this integrated CFD model, the effect of particle size on the attachment of highly floatable coal having a contact angle of 70^0 and 0.0527 m/s superficial air velocity is simulated. The predicted attachment fraction contours for the 40, 100, and 250 µm size particles are displayed in Fig. 10. It is found that the rate of attached particle fraction increases as the size increased from 40 to 100 µm. The model predicted a reduction in the attachment for the 250 µm sized particles. This trend is very consistent with the behavior of smooth spherical particles where the flotation rate found decreased for the coarser size particles, as reported by Schulze and Radoev (1989) & Koh & Schwarz (20006).

4. Conclusions

A CFD model was developed to predict the two-phase and three-phase hydrodynamics and kinetics of the column flotation. The average gas holdup values were predicted and validated with the Electrical Resistance Tomography (ERT) experimental data. The predicted CFD values are closely matching with the ERT data at low superficial air velocities and slight deviations are observed at high velocities. This

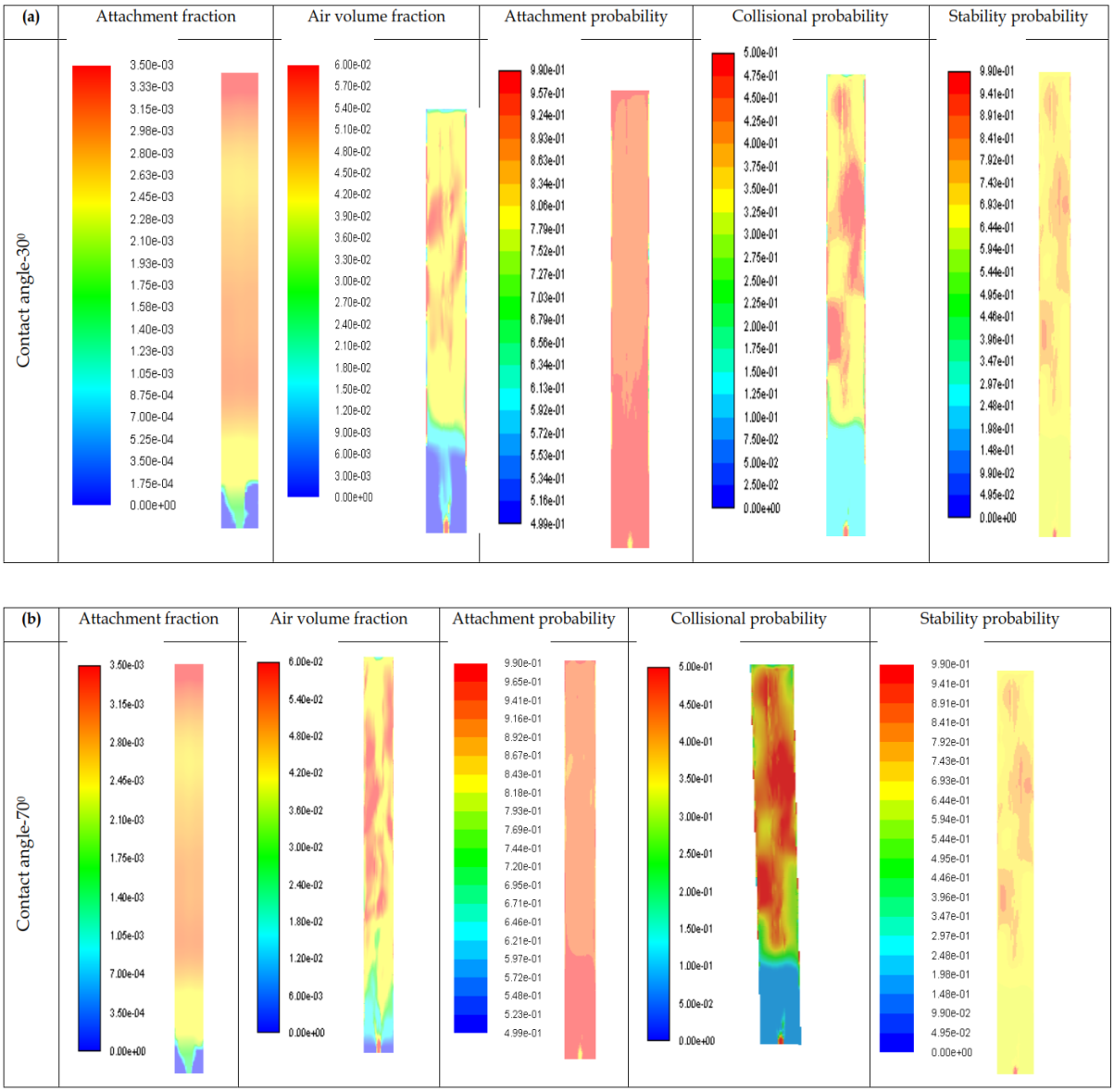

Fig. 8. Kinetic parameters and air volume fraction at (a) contact angle of 30^0 and (b) contact angle of 70^0

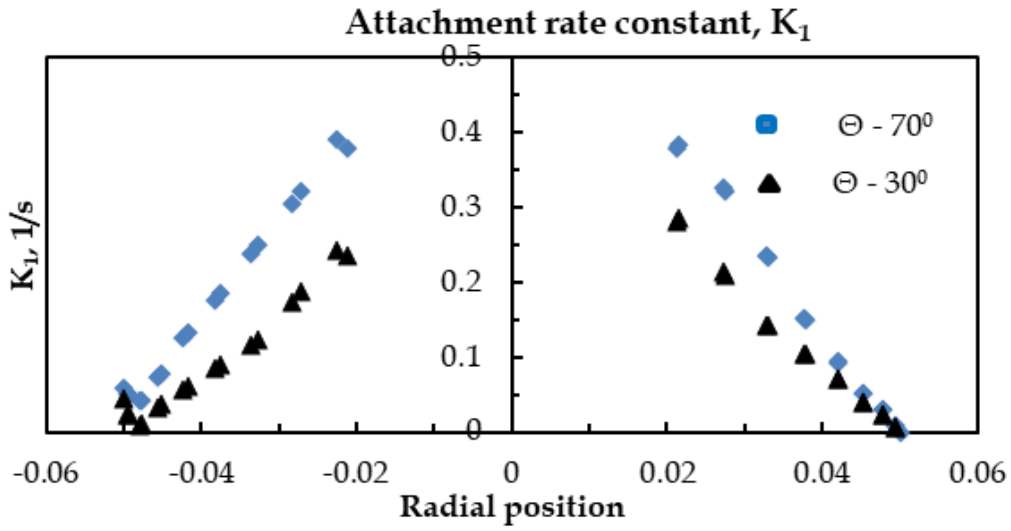

Fig. 9. Radial variation of bubble-particle attachment rate constant at a different contact angle

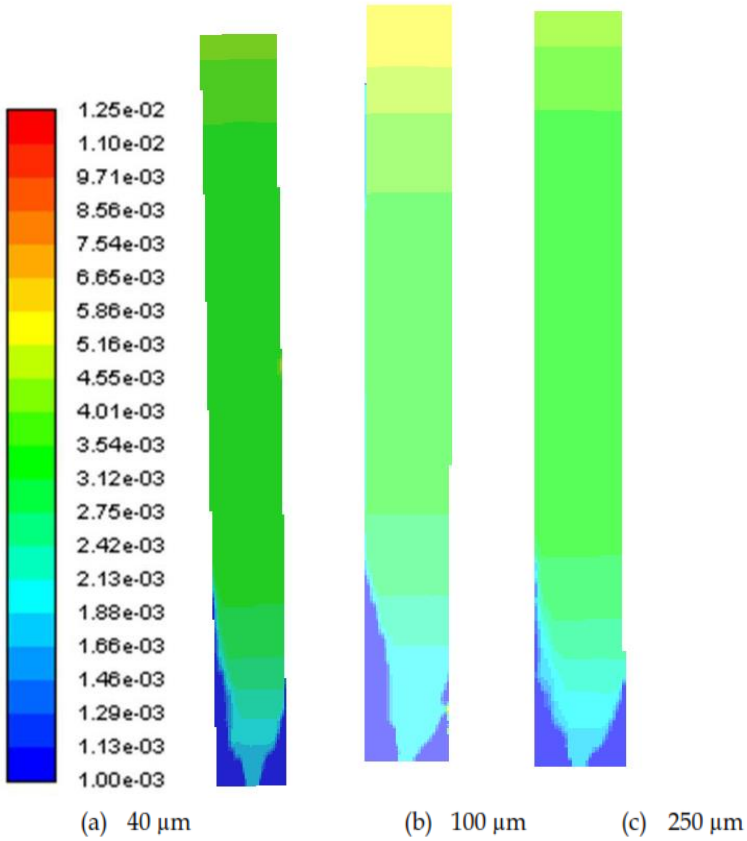

Fig. 10. Predicted particle attachment fraction for different size particles with a contact angle of 70^0

is due to the dominance of bubble break-up and coalescence phenomena at high air superficial velocities. In three phase study, both CFD predicted and experimental data demonstrated that the gas holdup decreased with solids content and increased with superficial air velocity. The error between the CFD predicted and the ERT experimental values for 5, 10, and 15 wt. % slurry solutions were 3.65, 7.10, and 7.55%, respectively at a superficial air velocity of 0.018 m/s. The rate constant was predicted using the Koh & Schwarz,(2006) approach, and the flotation sub-process such as bubble-particle collision, adhesion, and stability were also considered in the kinetic studies. The attachment rate constant values were found to increase with the contact angle. The increase in the hydrophobic nature of the particle results in to increase in the attachment fraction and a decrease in the detachment fraction. The simulation results were consistent with experimental values qualitatively. Further, the model simulated the flotation performance for different size particles and found that the rate of attached particle fraction increased from 40 to 100 µm and to slightly decreased for 250 µm, which is very consistent with the behavior of smooth fine and coarse spherical particle kinetic performance found in the literature.

Nomenclature

Nomenclature

$\overrightarrow{v_q}$ – the q^{th} phase velocity (m/sec)

$\vec{F}_q$ - an external body force (N)

$\vec{F}_{lift,q}$ - the lift force (N)

E_o - the Eotvos number $(E_o) = \frac{g\Delta\rho\, d_b^2}{\sigma}$ (dimensionless)

$E = \left[\frac{1+17.67(1-\alpha_q)^{\frac{6}{7}}}{18.67(1-\alpha_q)}\right]^2$ (dimensionless)

$E' = (1-\alpha_q)^2$ (dimensionless)

Greek letters

α_q – the q^{th} phase volume fraction (dimensionless)

ρ_q – the q^{th} phase density (kg/m^3)

$\bar{\bar{\tau}}_q$ - the q^{th} phase stress tensor (Pa)

φ_a - source term of attachment rate (1/s)

φ_d - source term of detachment rate. (1/s)

β - the average loading parameter (dimensionless)

$\vec{F}_{vm,q}$ – the virtual mass force (N)

$\vec{R}_{pq}$ – interaction force between phases(N)
$\vec{v}_{pq}$ – the interphase velocity (m/s)
p– the pressure shared by all phases (N/m^2)
N_{p1} - the number concentration of free particles (m^{-3})
N_{bT} - the total number of bubbles per unit volume (m^{-3})
k_1 - the particle-bubble attachment rate constant (1/s)
k_2 - the particle-bubble detachment rate constant(1/s)
n_{p2} – number density of attached particles (m^{-3})
d_{32} – Sauter mean diameter of bubbles, (m)
d_{sp} – diameter of solids particles, (m)
$\vec{u}_p$ – the turbulent (rms) fluctuating velocities of particles (m/s)
$\vec{u}_b$ – the turbulent (rms) fluctuating velocities of bubbles (m/s)
$d_{p,b}$ - diameter of solid particles or gas bubbles (m)
v_f - the kinematic viscosity of fluid (m^2/s)
u_f - mean fluctuating fluid velocity (m/s)
C_1 - an empirical constant with value 2 (dimensionless)
$u_{b,}$ - the bubble rise velocity (m/s)
t_{ind} - the induction time (sec)
C_L - lift coefficient(dimensionless)
C_{VM} - virtual mass coefficient(dimensionless)
$\vec{v}_p$ – particle velocity (m/s)

$\rho_{p,b}$ - densities of solid particles or gas bubbles (kg/m^3)
ρ_f – the density of fluid (kg/m3)
ε - local turbulent dissipation rate (m2/s3)
θ – Contact angle (^{0}).
μ_q – Shear viscosity of qth phase (Pa-s)
λ_q -Bulk viscosity of qth phase (Pa-s)
$I^=$ – the Kronecker delta (dimensionless)
ϑ– kinematic viscosity (m^2/s)

Acknowledgments

The authors would like to acknowledge IIT Hyderabad, the management of R&D TATA Steel for the encouragement and sponsoring of the joint research on CFD modelling studies of column flotation.

References

AHMED, N. & JAMESON, G.J., 1989. *Flotation Kinetics* Miner. Process. Extr. Metall. Rev. 5, 1–4, 77–99.

BANISI, S., FINCH, J.A., LAPLANTE, A.R., WEBER,M.E., 1995. *Effect of Solid Particles on Gas Holdup in Flotation Columns - I. Measurement* Chem. Eng. Sci. 50, 14, 2329–2334.

BHUNIA, K., KUNDU, G., MUKHERJEE,D., 2015. *Statistical model for gas holdup in flotation column in presence of minerals* Can. Metall. Q. 54, 2, 235–246.

FINCH, J.A. & DOBBY, G.S., 1990. *Column Flotation. Pergamon Press*, Oxford.

FINCH, J.A., XIAO, J., HARDIE,C., GOMEZ,C.O., 2000. *Gas dispersion properties: bubble surface area flux and gas holdup* Miner. Eng. 13, 4, 365–372.

HONAKER, R.Q. & MOHANTY, M.K., 1996. *Enhanced column flotation performance for fine coal cleaning* Miner. Eng. 9, 9, 931–945.

ISHII, M. & ZUBER, N., 1979. *Drag coefficient and relative velocity in bubble droplet or particulate flows*. AIChE J. 25, 5, 843–855.

KARIMI, M., AKDOGAN, G., BRADSHAW,S.M.,, 2014. *A computational fluid dynamics model for the flotation rate constant, Part I: Model development* Miner. Eng. 69, 214–222.

KOH, P.T.L. & SCHWARZ, M.P., 2003. *CFD modelling of bubble-particle collision rates and efficiencies in a flotation cell* Miner. Eng. 16, 11, 1055–1059.

KOH, P.T.L. & SCHWARZ, M.P., 2006. *CFD modelling of bubble-particle attachments in flotation cells* Miner. Eng. 19, 6–8, 619–626.

KOH, P.T.L. & SCHWARZ, M.P., 2008. *Modelling attachment rates of multi-sized bubbles with particles in a flotation cell* Miner. Eng. 21, 12–14, 989–993.

KOH, P.T.L., MANICKAM, M., SCHWARZ, M.P., 2000. *CFD Simulation of bubble- particle collisions in mineral flotation cells* Miner. Eng. 13, 14, 1455–1463.

LIEPE, F. & MOCKEL, H.O., 1976. *Studies of combinaiton of substtances in liqud phase 6, influence of turbulence on mass-transfer of suspended particles* Chem. Technol. 28, 205–290.

LIU, T.Y. & SCHWARZ, M.P., 2009. *CFD-based modelling of bubble-particle collision efficiency with mobile bubble surface in a turbulent environment* Int. J. Miner. Process. 90, 1–4, 45–55.

LUO, H., 1993. *Coalescence, breakup and liquid circulation in bubble column reactors. PHD thesis*, Norwegian Institute of Technology, Trondheim, Norway, 1993. 1993.

LUO, H. & SVENDSEN, H.F., 1996. *Theoretical model for drop and bubble breakup in turbulent* dispersions AIChE J. 42, 5, 1225–1233.

MENA, P.C., RUZICKA, M.C.,ROCHA,F.A.,TEIXEIRA,J.A.,DRAHOS,J., 2005. *Effect of solids on homogeneous-heterogeneous flow regime transition in bubble columns* Chem. Eng. Sci. 60, 22, 6013–6026.

MWANDAWANDE, I., AKDOGAN, G., BRADSHAW,S.M., KARIMI, M.,SNYDERS,N., 2019. *Prediction of gas holdup in a column flotation cell using computational fluid dynamics (CFD)* J. South. African Inst. Min. Metall. 119, 1, 81–95.

PANJIPOUR, R., KARAMOOZIAN, M., ALBIJANIC,B., 2021. *Investigations of gas holdup, interfacial area of bubbles and bubble size distributions in a pilot plant flotation column* Miner. Eng. 164, February, 106819.

PRAKASH, R., MAJUMDER, S.K., SINGH,A., 2018. *Flotation technique: Its mechanisms and design parameters* Chem. Eng. Process. - Process Intensif. 127, March, 249–270.

PYKE, B., FORNASIERO, D., RALTSON, J., 2003. *Bubble particle heterocoagulation under turbulent conditions* J. Colloid Interface Sci. 265, 1, 141–151.

SAFFMAN, P.G. & TURNER, J.S., 1956. *On the collision of drops in turbulent clouds* J. Fluid Mech. 1, 16–30.

SARHAN, A.R., NASER, J., BROOKS,G., 2016. *CFD simulation on influence of suspended solid particles on bubbles' coalescence rate in flotation cell* Int. J. Miner. Process. 146, 54–64.

SARHAN, A.R., NASER, J., BROOKS,G., 2017. CFD *Modeling of Three-phase Flotation Column Incorporating a Population Balance Model* Procedia Eng. 184, 313–317.

SCHULZE, H.J., RADOEV, B., 1989, I*nvestigation of the collision process between particles and bubbles,* International Journal of Mineral Processing, 27, 263-278.

SHAH, Y.T.,KELKAR, B.G., GODBOLE, S.P., 1982. *Design Parameters Estimations for Bubble Column Reactors. AIChE Journal* 28, 353–379.

SHUKLA, S.C., KUNDU, G., MUKHERJEE,D., 2010. *Study of gas holdup and pressure characteristics in a column flotation cell using coal* Miner. Eng. 23, 8, 636–642.

TAVERA, F.J. & ESCUDERO, R., 2002. *Gas holdu-up and solids hold-up in flotation columns:on-line measurement based on electrical conductivity* Miner. Process. Extr. Metall. Rev. 111, 2, 94–99.

TAVERA, F.J., ESCUDERO, R., FINCH, J.A., 2001. *Gas holdup in flotation columns: Laboratory measurements* Int. J. Miner. Process. 61, 1, 23–40.

VADLAKONDA, B. & MANGADODDY, N., 2017. *Hydrodynamic study of two phase flow of column flotation using electrical resistance tomography and pressure probe techniques* Sep. Purif. Technol. 184, 168–187.

VADLAKONDA, B. & MANGADODDY, N., 2018. *Hydrodynamic study of three-phase flow in column flotation using electrical resistance tomography coupled with pressure transducers* Sep. Purif. Technol. 203, June 2017, 274–288.

VAZIRIZADEH, A., BOUCHARD, J., DEL VILLAR, R., 2015. *On the relationship between hydrodynamic characteristics and the kinetics of column flotation. Part I: Modeling the gas dispersion* Miner. Eng. 74, 207–215.

YIANATOS, J., VINNETT, L., PANIRE,I., ALVAREZ-SILVA,M., DIAZ,F., 2017. *Residence time distribution measurements and modelling in industrial flotation columns* Miner. Eng. 110, January, 139–144.